JAMES | Journal of Advances in Modeling Earth Systems

RESEARCH ARTICLE
10.1029/2019MS002026

Special Section:
Geophysical Fluid Dynamics Laboratory CMIP6 Models

Ocean Ammonia Outgassing: Modulation by CO_2 and Anthropogenic Nitrogen Deposition

Fabien Paulot[1], Charles Stock[1], Jasmin G. John[1], Niki Zadeh[1,2], and Larry W. Horowitz[1]

[1]Geophysical Fluid Dynamics Laboratory, National Oceanic and Atmospheric Administration, Princeton, NJ, USA, [2]Science Applications International Corporation (SAIC), Reston, VA, USA

Abstract The imprint of anthropogenic activities on the marine nitrogen (N) cycle remains challenging to represent in global models, in part because of uncertainties regarding the source of marine N to the atmosphere. While N inputs of terrestrial origin present a truly external perturbation, a significant fraction of N deposition over the ocean arises from oceanic ammonia (NH_3) outgassing that is subsequently deposited in other ocean regions. Here, we describe advances in the Geophysical Fluid Dynamics Laboratory's (GFDL) Earth System Model 4 (ESM4.1) aimed at improving the representation of the exchange of N between atmosphere and ocean and its response to changes in ocean acidity and N deposition. We find that the simulated present-day NH_3 outgassing (3.1 TgN yr^{-1}) is 7% lower than under preindustrial conditions, which reflects the compensating effects of increasing CO_2 (−16%) and N enrichment of ocean waters (+9%). This change is spatially heterogeneous, with decreases in the open ocean (−13%) and increases in coastal regions (+15%) dominated by coastal N enrichment. The ocean outgassing of ammonia is shown to increase the transport of N from N-rich to N-poor ocean regions, where carbon export at 100 m increases by 0.5%. The implications of the strong response of NH_3 ocean outgassing to CO_2 for the budget of NH_3 in the remote marine atmosphere and its imprint in ice cores are discussed.

Key Points:
- Development of an interactive representation of N exchange between ocean and atmosphere in the GFDL ESM4.1, including ammonia outgassing
- Little change in the ocean NH_3 outgassing over the historical period due to compensation between acidification and increasing N deposition
- Ocean NH_3 outgassing increases carbon export at 100 m in N-limited regions by 0.5%

Supporting Information:
- Supporting Information S1

Correspondence to:
F. Paulot,
fabien.paulot@noaa.gov

Citation:
Paulot, F., Stock, C., John, J. G., Zadeh, N., & Horowitz, L. W. (2020). Ocean ammonia outgassing: Modulation by CO_2 and anthropogenic nitrogen deposition. *Journal of Advances in Modeling Earth Systems*, *12*, e2019MS002026. https://doi.org/10.1029/2019MS002026

Received 31 DEC 2019
Accepted 27 JUN 2020
Accepted article online 3 SEP 2020

1. Introduction

The availability of reactive nitrogen (N) limits the productivity of the ocean over much of the low-latitude oceans (Moore et al., 2013). This has motivated considerable research on the factors that control the supply of nitrogen to the euphotic zone. Across the global ocean, the dominant N source to the well-lit euphotic zone arises from the upward transport of N-rich subsurface waters via mixing or upwelling currents (e.g., Sarmiento & Gruber, 2013). However, lateral transport (e.g., Letscher et al., 2016), N deposition (e.g., Duce et al., 2008; Jickells et al., 2017), riverine inputs (e.g., Seitzinger et al., 2005), and nitrogen fixation (Wang et al., 2019) also play an important role at the regional level. Over the last 150 years, agricultural activities and fossil fuel combustion have led to a 4 times increase in N deposition to the ocean (Jickells et al., 2017). Models suggest that such increase in the N supply has resulted in significant changes in marine productivity both globally (+0.5% to 3% Duce et al., 2008; Jickells et al., 2017; Krishnamurthy et al., 2009) and regionally (Kim, Lee, Duce, et al., 2014; Krishnamurthy et al., 2010; St-Laurent et al., 2017). However, the response of the N cycle to increasing N deposition remains challenging to quantify. While field observations show that N availability in the northwest Pacific, in the immediate atmospheric outflow of East Asia, has increased, consistent with increasing N deposition (Kim et al., 2011; Ren et al., 2017), the extent to which it affects the open ocean remains uncertain (Kim, Lee, Gruber, et al., 2014; St-Laurent et al., 2017; Wang et al., 2018; Yang & Gruber, 2016). These discrepancies highlight ongoing challenges in characterizing the impacts of anthropogenic N deposition onto the marine N cycle.

A persistent source of uncertainty in current models is the representation of the marine source of atmospheric ammonia (NH_3) and organic nitrogen (Altieri et al., 2016; Jickells et al., 2017; Kanakidou et al., 2012; Wang et al., 2018). The ocean outgassing of ammonia is well supported by field observations (Gibb et al., 1999; Jickells et al., 2003; Johnson et al., 2007, 2008; Quinn et al., 1992, 1996) with recent studies suggesting that marine emissions could be the dominant source driving the gross deposition of $NH_x \equiv NH_3 + NH_4^+$ even in the outflow of continental sources (Altieri et al., 2014). The magnitude of the ocean source of NH_3 remains very uncertain with estimates ranging from 2 to 23 TgN yr^{-1} (Paulot et al., 2015). In most studies to date, marine NH_3 emissions are prescribed using a climatology (Bouwman et al., 1997). Such treatment does

not account for the bidirectional nature of NH_3 outgassing, which leads to an overestimate of the net N deposition to the ocean. The use of constant ocean NH_3 emissions also neglects changes in outgassing associated with changes in the sea water concentration of NH_3 due to climate change, acidification, and N deposition.

To reduce this uncertainty and elucidate the factors driving the response of marine NH_3 emissions to climate change in the Anthropocene, the Earth System Model 4 (ESM4.1) developed at the Geophysical Fluid Dynamics Laboratory (GFDL) includes a detailed representation of the atmospheric flux of nitrogen to the ocean, including the bidirectional exchange of NH_3 between ocean and atmosphere. This study is organized as follows. First, we document the representation of reduced nitrogen in the ocean biogeochemical component of ESM4.1 (Carbon, Ocean Biogeochemistry and Lower Trophics [COBALT]) and its coupling with N deposition. We focus on changes to the representation of nitrification and uptake by phytoplankton and its impact on the simulation of surface $[NH_x(sw)]$. We then characterize the magnitude of ocean outgassing and its response to changes in N deposition and CO_2 over the 1850–2014 period. We conclude by discussing how the sensitivity of NH_3 emissions to CO_2 affects the concentration of NH_3 in the remote atmosphere and its imprint in ice cores.

2. Model Formulation

The main characteristics of GFDL-ESM4.1 are described in detail in Dunne et al. (2020) and in Adcroft et al. (2019), Zhao et al. (2018), Stock et al. (2020), and Horowitz et al. (2020) for the overall coupled, ocean dynamics, atmospheric dynamics, ocean biogeochemistry, and atmospheric chemistry components, respectively. The nominal horizontal resolution of the atmosphere and ocean models are ≃100 km and 0.5°, respectively.

We focus here on the simulation of surface seawater ammonia $NH_x(sw) \equiv NH_3(sw) + NH_4^+(sw)$ and the representation of atmospheric N deposition to the ocean including the bidirectional exchange of atmospheric NH_3.

Analysis of the model performance is based on the historical simulation averaged over three ensemble members from 1990 to 2014. Changes in the N deposition and NH_3 outgassing are analyzed relative to the first 400 years of the preindustrial control (piControl) simulation and years 24 to 34 of a simulation with CO_2 increasing at $1\%\,yr^{-1}$ (1pctCO2), chosen to match the CO_2 concentration over the 1990–2014 period.

2.1. $NH_x(sw)$ Budget in COBALTv2

Ocean biogeochemistry in ESM4.1 is simulated with version 2 of the COBALT model (COBALTv2, Stock et al., 2020). In COBALTv2, sources of $NH_x(sw)$ are dominated by biological remineralization (≃10 PgN yr^{-1}) with minor contributions from NH_x deposition. Excretion of ammonium is associated with respiration of organic carbon following OCMIP-II biotic protocols (Anderson, 1995). Respiration and ammonium excretion is thus associated with feeding by all zooplankton, free living bacteria remineralizing dissolved organic material, implicit particle-attached bacteria remineralizing sinking detritus, and implicit "fish" predators consuming zooplankton. Excretion also occurs in COBALTv2 when net phytoplankton growth becomes negative (i.e., under low light conditions). More details can be found in Stock et al. (2020).

Sinks of $NH_x(sw)$ include nitrification (≃25%) and uptake by phytoplankton (≃75%). Anammox is not represented in COBALTv2 (Gruber, 2008). We focus here on the changes in the representation of the NH_x sink between COBALTv1 and COBALTv2. Nitrification (*jnitrif*) is parameterized as

$$\begin{aligned} jnitrif &= \gamma_{nitrif} \cdot f_T \cdot f_{\text{light}} \cdot f_{O_2} \cdot f_{NH_3} \cdot [NH_x(sw)]^b \quad \text{if } [O_2] > [O_{\min}] \\ &= 0 \text{ otherwise} \end{aligned} \tag{1}$$

with

$$f_T = exp(k_T T) \tag{2}$$

$$f_{\text{light}} = \left(1 - \frac{I_{24}}{I_{24} + IRR}\right) \tag{3}$$

Table 1
Parameter Values Used in COBALTv2

Parameter	Value
γ_{nitrif}	1.35 kg mol^{-1} s^{-1}
$\kappa^{nitrif}_{NH_3}$	3.1 nmol kg^{-1}
k_{O_2}	3.9 μmol kg^{-1}
k_T	0.063 °C^{-1}
IRRI	10 W m^{-2}
b	2
κ_{NH_x} (small phytoplankton)	10^{-5} mmol kg^{-1}
κ_{NH_x} (large phytoplankton)	5×10^{-5} mmol kg^{-1}
κ_{NH_x} (diazotroph)	1×10^{-4} mmol kg^{-1}
$\kappa_{NO_3^-}$ (small phytoplankton)	5×10^{-4} mmol kg^{-1}
$\kappa_{NO_3^-}$ (large phytoplankton)	25×10^{-4} mmol kg^{-1}
$\kappa_{NO_3^-}$ (diazotroph)	5×10^{-3} mmol kg^{-1}

$$f_{O_2} = \frac{[O_2]}{k_{O_2} + [O_2]} \tag{4}$$

$$f_{NH_3} = \frac{[NH_3(sw)]}{[NH_3(sw)] + \kappa^{nitrif}_{NH_3}} \tag{5}$$

f_T and f_{O_2} reflect the sensitivity of nitrification to temperature (T) and oxygen (O_2) with k_T and k_{O_2} given in Table 1. f_{light} represents the inhibition of nitrification by light (Ward et al., 1982) with *IRRI* and I_{24}, the light inhibition threshold (Table 1) and the 24-hr mean light irradiance, respectively. γ_{nitrif} is a normalization factor. The sensitivity to light and O_2 is reduced relative to COBALTv1 following Peng et al. (2016) and Smith et al. (2014). Unlike COBALTv1, we account for the sensitivity of nitrification to the speciation of NH_x via f_{NH_3} (Beman et al., 2011; Huesemann et al., 2002; Kitidis et al., 2011; Stein et al., 1997; Suzuki et al., 1974; Ward, 2008). This introduces an additional modulation of nitrification by acidification (decrease) and warming (increase) through the pKa of NH_4^+/NH_3 (Clegg & Whitfield, 1995). COBALTv2 does not explicitly represent nitrifying organisms, and we set $b = 2$ to represent the adjustment of the biomass of nitrifying organisms to NH_4^+ availability. Tuning of γ_{nitrif} is based on surface NH_x observations, and further assessment against a compilation of nitrification rates is currently underway.

The uptake of NH_x by phytoplankton is controlled by the N required to support growth rates achieved under prevailing nutrient and light conditions (Geider et al., 1997; Stock et al., 2020) and their relative preference for NH_x relative to NO_3^- (Dortch, 1990; Glibert et al., 2015; Syrett, 1981). COBALTv2 allows for the inhibition of the uptake of NO_3^- and NH_x in the presence of abundant NH_x and NO_3^-, respectively, following O'Neill et al. (1989):

$$\frac{j_{NH_x}}{j_{NO_3^-}} = \frac{[NH_x(sw)]}{\kappa_{NH_x} + [NH_x(sw)] + \frac{\kappa_{NH_x}}{\kappa_{NO_3^-}}[NO_3^-(sw)]} \frac{\kappa_{NO_3^-} + [NO_3^-(sw)] + \frac{\kappa_{NO_3^-}}{\kappa_{NH_x}}[NH_x(sw)]}{[NO_3^-(sw)]} \tag{6}$$

where j_X denotes the uptake rate of X and the half-saturation for NO_3^- ($\kappa_{NO_3^-}$) and NH_x (κ_{NH_x}) are given in Table 1. We note that the O'Neill et al. (1989) parameterization results in less inhibition of NO_3^- uptake by NH_x than the parameterization of Frost and Franzen (1992) that was used in previous versions of the model (ESM2M-COBALT, Paulot et al., 2015; Stock et al., 2014a), particularly in iron-limited high-nutrient low-chlorophyll (HNLC) areas where NO_3^- is found in abundance. The impact of changes in the nitrification and ammonium uptake scheme on the simulation of $NH_x(sw)$ will be discussed in section 3.1.

2.2. Atmosphere-Ocean N Exchange

2.2.1. NH_3 Exchange

The net exchange of NH_3 (F) between ocean and atmosphere is calculated following Liss and Slater (1974) as described in Paulot et al. (2015).

$$F = -K([NH_3] - H^\star[NH_x(sw)]) \tag{7}$$

where $H^\star$ is the dimensionless effective Henry's law constant for NH_x and K is the transfer velocity between atmosphere and ocean.

$$H^\star = \frac{H}{1 + 10^{-pH + pKa_{NH_3}}} \tag{8}$$

$$K = \left[\frac{1}{k_g} + \frac{H}{k_w}\right]^{-1} \tag{9}$$

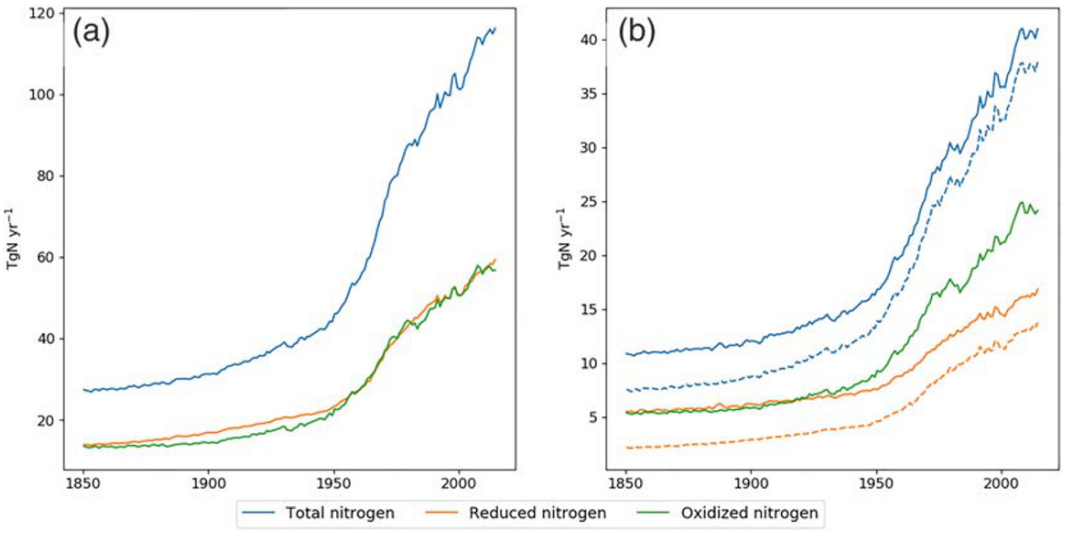

Figure 1. Historical changes in speciated global N emissions (a). Simulated N deposition to the ocean (b). Dashed lines show the net deposition.

where H is the Henry's law constant for NH_3 (Jacobson, 2005), pKa_{NH_3} is the $-\log_{10}$ of the acid dissociation constant of NH_3/NH_4^+ (Clegg & Whitfield, 1995), and k_g and k_w are the transfer velocities in the gas phase and water, respectively (Johnson, 2010). For NH_3, $K \simeq k_g$ under environmentally relevant conditions (Beale et al., 2014). k_g is calculated following Johnson (2010):

$$k_g = 10^{-3} + \frac{u_\star}{13.3\sqrt{Sc_a} + C_D^{-1/2} - 5 + \frac{ln(Sc_a)}{2\kappa}} \tag{10}$$

where Sc_a is the airside Schmidt number, C_D is the drag coefficient, $u_\star$ is the friction velocity, and κ is the von Karman constant ($\kappa = 0.4$).

In our previous work (Paulot et al., 2015), we used a climatology for $[NH_x(sw)]$ derived from ocean biogeochemical models including ESM2M-COBALT. Here, the atmospheric and ocean pools of NH_3 are coupled and simulated interactively. In this way, $NH_x(sw)$ responds to NH_3 outgassing and its impact on ocean biogeochemistry can be quantified.

2.2.2. Other Atmospheric Sources of Nitrogen

ESM4.1 includes a detailed representation of the atmospheric chemistry of NH_x and NO_y (Horowitz et al., 2020). Emissions of reactive nitrogen include anthropogenic emissions from the Community Emissions Data System v2017-05-18 (Hoesly et al., 2018) and biomass burning emissions (BB4CMIP, van Marle et al., 2017). Surface natural sources of NH_3 and NO are prescribed following Naik et al. (2013) for soil and land-based animals and Riddick et al. (2012) for sea bird NH_3 emissions. NO emissions from lightning are calculated following Naik et al. (2013). Ammonia partitioning between aerosol and gas phase is determined using the thermodynamic model ISORROPIA (Fountoukis & Nenes, 2007) as described in Paulot et al. (2016). Removal rates of oxidized and reduced nitrogen by wet and dry deposition are calculated in the atmospheric component of ESM4.1 and passed to COBALTv2 every hour (the ocean coupling time step). This treatment improves the representation of the spatial and temporal variability of N deposition relative to ESM2M-COBALT for which a climatology of N deposition was used (Stock et al., 2014b).

Figure 1a shows the simulated changes in global reactive N emission over the 1850–2014 period, and Figure 1b shows the associated change in marine N deposition. Total emissions increase from 27.4 to 116 TgN yr^{-1} from 1850 to 2014 with comparable contributions from oxidized and reduced nitrogen. Our estimates are $\simeq$20 TgN yr^{-1} lower than in the study of Jickells et al. (2017), which is consistent with the incomplete representation of organic nitrogen in ESM4.1. Gross and net marine N deposition increase from 11 to 41 and from 7.5 to 38 TgN yr^{-1}, respectively. Table 2 shows that the net total and reduced N deposition to the

Table 2
Simulated Net N Deposition Under Preindustrial (PI) and Present-Day (PD; 1990–2014) Conditions (in TgN yr^{-1})

	N deposition		NH_x deposition	
	PI	PD	PI	PD
All ocean	7.5	34.3	2.2	12.1
Open ocean	4.3	15.7	0.9	5.1
Coastal regions	3.2	18.7	1.2	7
Asia[a]	0.9	7.0	0.4	2.9
Contiguous United States[b]	0.1	1.3	0.04	0.3
Europe[c]	0.3	2.3	0.2	0.9

[a]Red Sea, Bay of Bengal, Gulf of Thailand, South and East China Seas, Yellow Sea, Kuroshio Current, Sea of Japan. [b]North and Baltic Seas, Celtic-Biscay Shelv, Iberian Coastal, and Mediterranean. [c]California Current, Gulf of Mexico, Southeast and Northeast U.S. Continental Shelves.

oceans have increased by 4.6 and 5.6 times, respectively. Over 50% of present-day N deposition occurs in coastal areas, defined here as large marine ecosystems (LMEs, Sherman & Alexander, 1986), with coastal Asia, Europe, and the United States accounting for more than 30% of all N deposition to the ocean. The largest fractional increase is simulated in North American coastal water (11 times, including 22 times for the Northeast U.S. continental shelf). Approximately 40% of emitted oxidized nitrogen is deposited over the ocean, where it accounts for over 60% of the gross marine N deposition to both coastal and open ocean.

3. Results and Discussion

3.1. Evaluation of $NH_x(sw)$ Concentration

There is currently no global database of $[NH_x(sw)]$, which complicates model evaluation. Here, we use surface $[NH_x(sw)]$ observations (depth < 10 m) summarized by Paulot et al. (2015) supplemented by observations from the Climate and ocean-variability, predictability, and change and Carbon Hydrographic Data Office (CCHDO) and SeaDataNet. We exclude observations exceeding 2 mmol m^{-3} to reduce the influence of coastal hot spots. After filtering, the median $[NH_x(sw)]$ is 0.13 mmol m^{-3}. We note that the detection threshold for conventional colorimetric techniques (≃0.08 mmol m^{-3}) is higher than the simulated $[NH_{sw}]$ in many oligotrophic regions, which may cause a positive bias.

In Paulot et al. (2015), we reported that the simulated $[NH_x(sw)]$ in the ESM2M-COBALT model was biased high and we increased phytoplankton's affinity for $NH_x(sw)$ to reduce this bias. Figure S1 shows that the resulting configuration (ESM2M-COBALT-HA) exhibits low normalized mean bias (NMB) in all seasons ($|NMB| \leq 20\%$), where NMB is estimated as 10^{Δ} with Δ the difference between the $\log_{10}$ of the simulated and observed surface $[NH_x(sw)]$. However, ESM2M-COBALT-HA does not capture the spatial distribution of $[NH_x(sw)]$ well with R ranging from 0.17 to 0.4. Figure 2 shows that ESM4.1 captures the spatial distribution of $[NH_x(sw)]$ better, with correlations ranging from 0.48 to 0.52 on a seasonal basis, without significant increase in the model bias ($|NMB| \leq 25\%$). In particular, ESM4.1 better captures the observed elevated $[NH_x(sw)]$ in the Southern Ocean in DJF and MAM. This improvement is primarily driven by the reduced

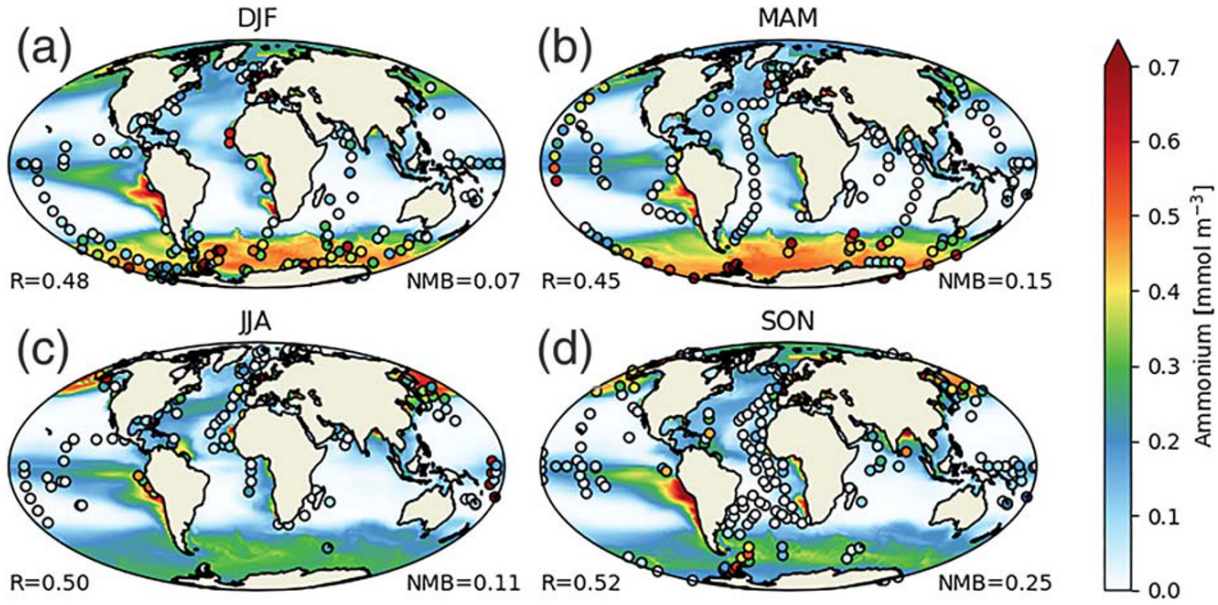

Figure 2. Seasonal mean surface seawater concentration of total ammonium ($NH_x(sw)$) simulated by ESM4.1 (1990–2014 average). Observations are denoted by circles and averaged onto a 7.5 × 7.5° grid for readability. Normalized mean biases (NMBs) and correlation (R) are indicated in the insets.

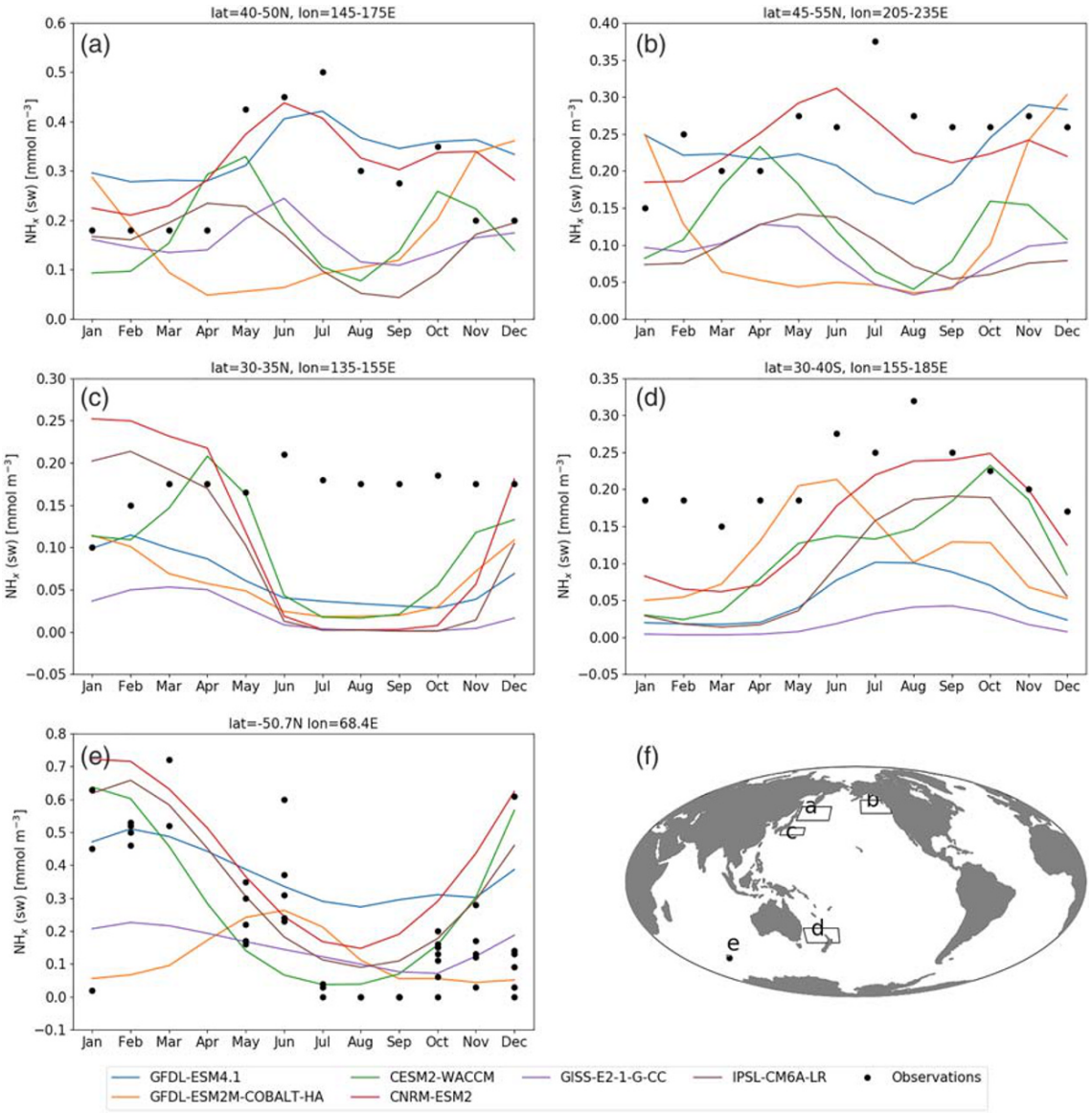

Figure 3. Comparison between observed (dots) and simulated surface $NH_x(sw)$ from ESM2M-COBALT-HA, ESM4.1, and other CMIP6 models. Observations are from Yasunaka et al. (2017) (a–d) and Jeandel et al. (1998) (e). The location of the different regions is shown in panel (f).

preference of phytoplankton for $NH_x(sw)$ at high $[NO_3^-(sw)]$ (Glibert et al., 2015; as parameterized in O'Neill et al., 1989).

Comparisons against the few available time series of surface $[NH_x]$ also show improvements in the seasonality of $NH_x(sw)$ at high latitudes relative to ESM2M-COBALT-HA (Figure 3). However ESM4.1 tends to underestimate the post-bloom decrease of $NH_x(sw)$ in the Southern Ocean (Figure 3e), suggesting that the decrease of nitrification with temperature (both through k_T and f_{NH_3}) needs to be revisited. Figure 3 also shows the simulated surface concentrations of NH_x in five CMIP6 models averaged over 1990 to 2014. Large differences in both the magnitude and the seasonality of $NH_x(sw)$ across models highlight continuing challenges in the representation of NH_x in models (Paulot et al., 2015), which are compounded by sparse measurements of patchy NH_x fields. The large difference in the simulated seasonality of NH_x in midlatitudes across CMIP6 models (Figures 3a and 3b) is consistent with that between ESM2M-COBALT-HA and ESM4.1, suggesting that it may be associated with similar differences in the treatment of nitrification and ammonium uptake across CMIP6 models.

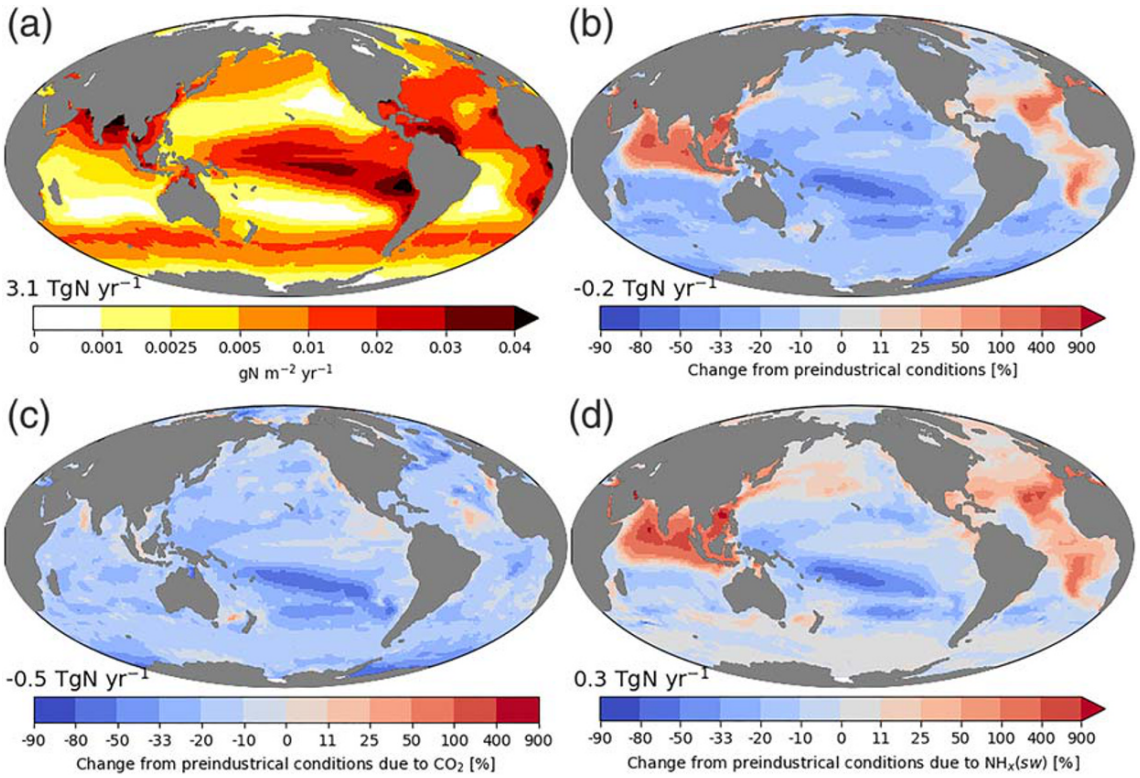

Figure 4. 1990–2014 average simulated ocean NH_3 outgassing (a) and its relative change from preindustrial conditions (b). Relative changes in ocean NH_3 outgassing due to changes in CO_2 and $NH_x(sw)$ between preindustrial and present-day conditions are shown in panels (c) and (d), respectively. The magnitude of NH_3 outgassing (a) and its change (b–d) are indicated in inset.

3.2. Susceptibility of Ocean Ammonia Outgassing to N Deposition and Climate Change

Figure 4a shows the distribution of ocean outgassing in present-day conditions. The magnitude of NH_3 outgassing in ESM4.1 is 3.1 TgN yr^{-1} under present-day conditions, similar to estimates derived by Paulot et al. (2015) (2–5 TgN yr^{-1}) but much lower than estimates commonly used in global models (8.2 TgN yr^{-1}) (Bouwman et al., 1997; Jickells et al., 2017). The spatial distribution of ocean NH_3 outgassing reflects both the distribution of $[NH_x(sw)]$, with high emissions from N-rich upwelling regions, iron-limited HNLC regions (e.g., equatorial Pacific, Southern Ocean, and North Pacific), and river outflows (e.g., Amazon, Congo, Indus), as well as the sensitivity of NH_3 solubility to sea surface temperature, which results in higher emissions in the equatorial Pacific than in the Southern Ocean. The large outgassing of NH_3 in the equatorial Pacific is consistent with recent isotopic measurements (Kamezaki et al., 2019) that suggest that a significant portion of NO_x in this region may be derived from the oxidation of marine N.

ESM4.1 simulates a small decrease ($\simeq$7%; Table 3 and Figure 4b) in NH_3 outgassing from preindustrial conditions to 1990–2014 conditions, with contrasting changes in coastal regions (increase) and open ocean (decrease). Figure 4c shows that changes in CO_2 alone (estimated from the 1pctCO2 simulation averaged from years 24 to 34 to match CO_2 concentrations over the 1990–2014 period) would result in a stronger decline in NH_3 outgassing (-16%, Table 3). This change is consistent with the decrease in the $NH_3(sw)$: $NH_x(sw)$ ratio ($\simeq -17\%$) associated with the change in surface pH from 8.17 in 1850 to 8.09 over the 1990–2014 period. The difference between the CO_2-alone response and the historical response can be well explained by changes in $[NH_x(sw)]$, particularly in coastal areas strongly impacted by increasing deposition, which has led to an increase in NH_3 outgassing of 0.3 TgN yr^{-1}, thus offsetting more than half of the changes induced by acidification (Figure 4). The decrease of ocean outgassing in the subtropical South Pacific is due to changes in both CO_2 and $[NH_x(sw)]$ consistent with a reduction in $[NH_x(sw)]$ from increased stratification (Capotondi et al., 2012).

Table 3
Regional Changes in NH_3 Outgassing (in TgN yr^{-1})

	Present-day outgassing	Change from preindustrial		
		Overall (%)	Due to CO_2 (%)	Due to NH_x (%)
All ocean	3.1 (2.4)	−7	−16	+9
Open ocean	2.3 (1.9)	−13	−17	0
Coastal regions	0.8 (0.5)	+15	−12	+38
Asia	0.22 (0.12)	+62	−13	+120
Contiguous United States	0.05 (0.02)	+6.5	−14	+26
Europe	0.03 (0.03)	+31	−17	+55

Note. Regions are the same as in Table 2. Emissions from ESM2M-COBALT-HA are indicated in parentheses (Paulot et al., 2015; Stock et al., 2014b).

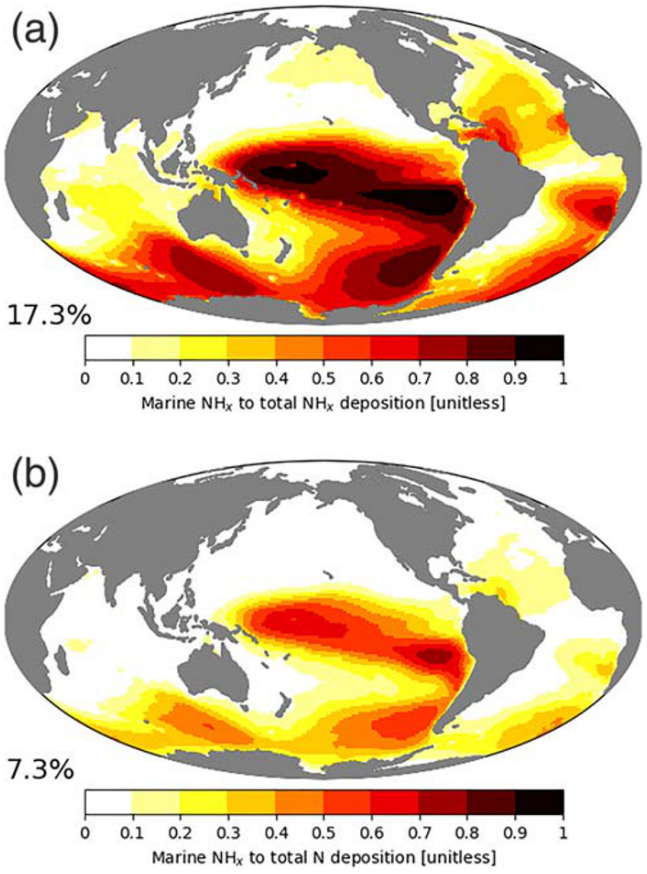

Figure 5. Contribution of marine NH_x deposition to total NH_x (a) and N deposition (b). The global contributions are indicated in insets. The location of Bermuda is indicated by a black dot.

The opposing responses of NH_3 outgassing to N deposition and acidification help explain the contrasting response of NH_3 outgassing in coastal regions and in the open ocean. In the open ocean, ESM4.1 simulates a 13% decrease in NH_3 outgassing. This is consistent with the impact of CO_2 alone (−16%) and the small impact of N deposition on open ocean [$NH_x(sw)$] (Table 3). In contrast, coastal NH_3 outgassing has increased by 15% from preindustrial conditions to present day, as the increase in $NH_x(sw)$ outweighs the impact of acidification. The increase in coastal NH_3 outgassing is likely to be underestimated in ESM4.1, as riverine N concentrations are held at constant contemporary values (Seitzinger et al., 2005) throughout the simulation. The relative change in outgassing ranges from +6.5% off the coast of the contiguous United States to 62% off the coast of Asia, which is consistent with changes in absolute N deposition to these regions. The compensation between acidification and N deposition also has implications for future NH_3 outgassing. At CO_2 doubling, the simulated NH_3 outgassing is 2.78 TgN yr^{-1} under the Shared Socioeconomic Pathways scenario 3-7.0 (Fujimori et al., 2017) but 1.86 TgN yr^{-1} with CO_2 increase alone (Figure S2). This suggests that N deposition can offset almost two thirds of the impact of CO_2 on ocean NH_3 outgassing.

Differences between the responses of coastal and open-ocean NH_3 outgassing in ESM4.1 are also useful to understand differences between ESM2M-COBALT-HA and ESM4.1 (+35%, Table 3). Open-ocean outgassing is 20% greater in ESM4.1, which reflects changes in [$NH_x(sw)$] associated with the updated treatment of ammonium uptake and nitrification (Figures 2 and S1). The difference is much larger for coastal outgassing (+60%) and similar to the simulated change in outgassing due to $NH_x(sw)$ between preindustrial and present day in ESM4.1 (+38%). This is consistent with the fact that ESM2M-COBALT-HA does not consider the increase of N deposition between preindustrial and present day. We note that there remain important uncertainties in the simulated response to increasing N deposition. For instance, higher outgassing in the Arabian Sea, Bay of Bengal, Northwest Pacific, and North Atlantic is stimulated by a simulated shift toward phosphate limitation in these regions in response to increasing anthropogenic N inputs. While there is evidence for growing phosphate limitations in these regions (e.g., Kim, Lee, Gruber, et al., 2014; Martiny et al., 2019 and references therein), it is likely overexpressed in ESM4.1 (Stock et al., 2020).

3.3. Impact of NH_3 Exchange Under Present-Day Conditions

To quantify the impact of changes in ocean NH_3 outgassing, we perform a sensitivity experiment, in which the outgassing of NH_3 is suppressed. Three ensemble members were branched from the historical simulations starting in 1970 and analyzed over the 1990–2014 period. Comparison of the deposition with bidirectional exchange suppressed to deposition when included quantifies the relative importance of marine-derived NH_x deposition to the total deposition for the whole ocean and for each region.

Figure 5 shows that NH_3 outgassing accounts for ≃17% and 7% of the total gross marine deposition of NH_x and N, respectively, over the 1990–2014 period (Figure 5). The contribution of marine NH_3 emissions exceeds 50% in remote regions such as the equatorial Pacific and Southern Ocean. The ocean contributes little to N deposition in the outflow of

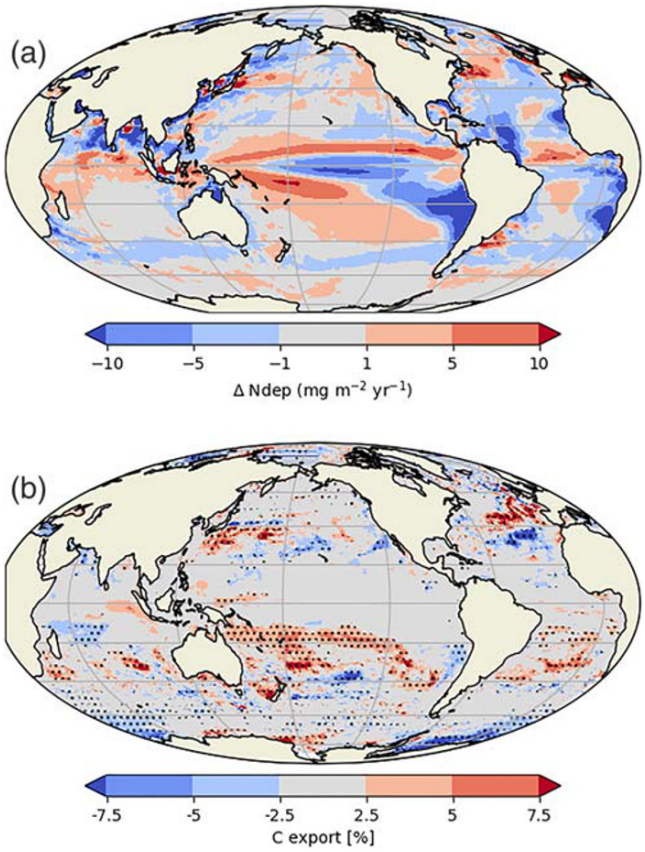

Figure 6. Changes in net N deposition (1990–2014) associated with ocean ammonia outgassing and its impact on the carbon export at 100 m (b). Regions where changes are statistically significant ($p < 0.1$) are denoted by dots.

North America, Asia, and Europe. For instance, the ocean is simulated to contribute 20–35% of the annual NH_x deposition at Bermuda (32.3°N, 64.9°W). This disagrees with isotopic constraints, which suggest that most NH_x deposited at this location is of marine origin (Altieri et al., 2014). Part of the discrepancy may reflect the release of ammonia from the photochemical degradation of organic nitrogen (Paulot et al., 2015; Zhang & Anastasio, 2003); marine emissions of which are not included in our calculations but may exceed direct marine NH_3 emissions (Jickells et al., 2017; Kanakidou et al., 2012).

Figure 6a shows that NH_3 outgassing tends to transport marine nitrogen away from N-rich regions ($\Delta Ndep < 0$), such as upwelling regions, HNLC regions, and river outflows (e.g., Amazon, Congo, Indus), to regions with low NH_3 partial pressures. The atmospheric redistribution of marine nitrogen via NH_3 outgassing results in statistically significant increases in carbon export at 100 m ($p < 0.1$) in much of the South Pacific and South Atlantic gyres, where changes can exceed 5% (Figure 6b). Overall, we find that the carbon export at 100 m in regions of low NO_3^- concentration (annual mean $NO_3^- < 2$ mmol m^{-3}) increases significantly (+0.5%, $p < 0.1$). Changes in N deposition associated with the atmospheric redistribution of outgassed NH_3 are accompanied by opposite changes in N fixation in the Southern Pacific, Indian Ocean, and Southern Ocean (Figure S3). This change in N fixation may partly reduce the impact of the redistribution of outgassed NH_3 on ocean biogeochemistry, as previously noted for anthropogenic N deposition (Krishnamurthy et al., 2007, 2009).

3.4. Implication for the Remote Budget of NH_3

Figure 7a shows the response of ocean NH_3 outgassing to a doubling of CO_2. The global outgassing is reduced more (−42%) than expected from changes in surface pH alone ($\simeq -33\%$). This can be attributed to increasing stratification and accompanying primary production declines (Stock et al., 2020), which exacerbates the decline of NH_3 outgassing. In contrast, NH_3 outgassing increases in boreal regions, which reflects the reduction in sea ice cover. The overall reduction in NH_3 outgassing is accompanied by a decrease in the concentration of near-surface atmosphere NH_3 (Figure 7b). This reduction is especially large in the equatorial Pacific, where preindustrial NH_3 emissions are sufficient to neutralize non-sea salt sulfate (nss-SO_4^{2-}). In contrast, little change is simulated in polar regions, as the increase in NH_3 emissions remains insufficient to neutralize nss-SO_4^{2-}. Regional differences in the gas/aerosol partitioning of NH_3 remain challenging to verify because of limited observations of atmospheric NH_3 in remote regions (Paulot et al., 2015). In addition, changes in Dimethyl sulfate (DMS) emissions, the primary source of non-sea salt sulfate in the remote marine atmosphere, with global warming and acidification (Hopkins et al., 2020), may further modulate the response of atmospheric NH_3 to climate change. Such changes are not considered in ESM4.1.

Finally, we note that changes in marine NH_3 outgassing with CO_2 may also help interpret changes in ice core NH_4^+ in Antarctica. In this region, 50–70% of NH_x deposition is simulated to originate from the ocean, which agrees well with limited in situ constraints (Kaufmann et al., 2010; Legrand et al., 1998). Figure 7c shows that the decrease in NH_3 outgassing associated with a doubling of CO_2 leads to a 20–35% decline in NH_x concentration in precipitation over most of Antarctica. The decrease of NH_3 outgassing with ocean acidification may thus be an important driver for the 70% lower NH_4^+ concentration in the ice cores collected by European Project for Ice Coring in Antarctica (Kaufmann et al., 2010) at the beginning of the last glacial period ($CO_2 \simeq 253$ ppmv) relative to the last glacial maximum ($CO_2 \simeq 188$ ppmv). We further note that our simulations do not support a correlation between NH_x in ice cores and the productivity of the Southern Ocean as hypothesized by Kaufmann et al. (2010).

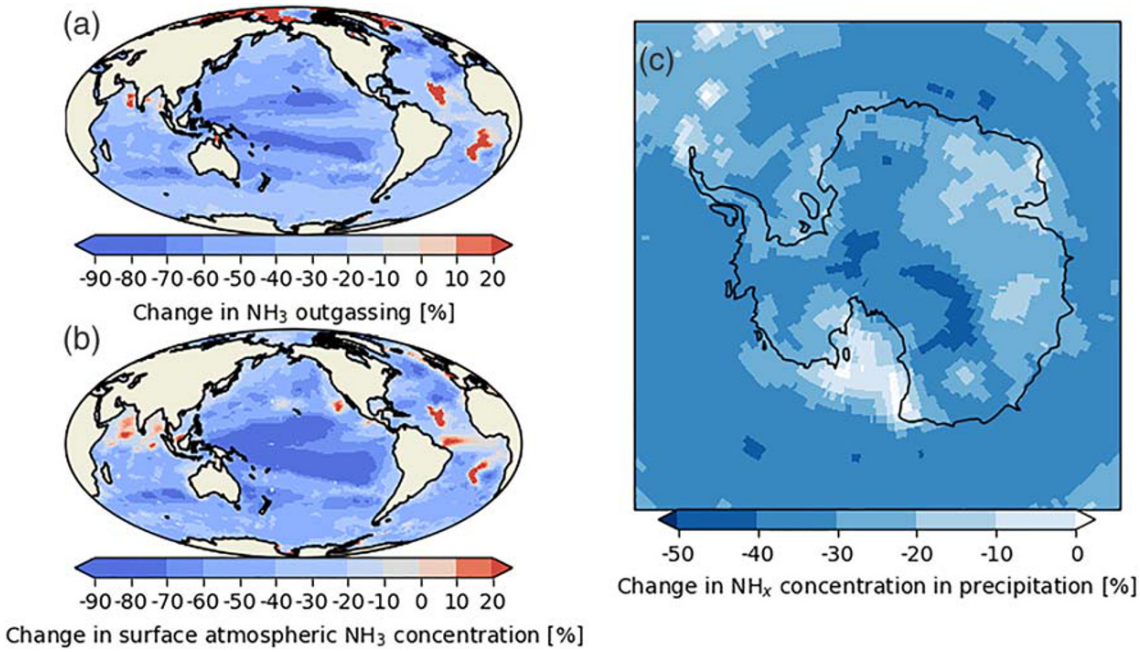

Figure 7. Relative response of NH_3 outgassing (a), near-surface atmospheric NH_3 concentration (b), and NH_x deposition (c) to a doubling of atmospheric CO_2.

4. Conclusions

ESM4.1 implements a comprehensive representation of N exchange between the ocean and atmosphere. Our estimate of global marine NH_3 emissions (3.1 TgN yr^{-1}) falls within the range estimated by Paulot et al. (2015) (2–5 TgN yr^{-1}) using a previous version of the model, despite large changes in the model physics and treatment of $NH_x(sw)$. Small changes in ocean NH_3 outgassing simulated over the historical period (−7%) reflect the competition between ocean acidification (−16%) and N deposition (+9%). The impact of N deposition on ocean outgassing is most important in coastal regions, where a 15% increase in NH_3 outgassing is simulated. Ammonia outgassing contributes to the supply of N to N-poor area, where it promotes carbon export at 100 m (≃+0.5%).

Ammonia outgassing is projected to decrease by 42% in response to a doubling of CO_2 primarily due to acidification, with a greater decrease in subtropical regions due to lower primary production associated with higher stratification. This reduction in ocean ammonia outgassing results in a large decrease (70%) in near-surface atmospheric NH_3 in the equatorial and subtropical Pacific, which may impact aerosol pH and aerosol nucleation (Dunne et al., 2016; Jokinen et al., 2018; Kirkby et al., 2011). We further suggest that the decrease of NH_3 ocean outgassing with increasing CO_2 can also explain most of the increase in the concentration of NH_x in Antarctic ice cores between 125 and 22.5 kyr BP (Kaufmann et al., 2010).

Finally, we suggest that the following items should be prioritized to help reduce the uncertainty in the magnitude and sensitivity of NH_3 outgassing that is reflected in the considerable range of estimates for NH_3 outgassing (2–23 TgN yr^{-1}).

1. Development of a global database of quality-controlled surface $NH_x(sw)$ observations. This is especially important in oligotrophic regions, where $NH_x(sw)$ concentrations are often below detection limit for conventional colorimetric techniques. Such a database was recently developed by Yasunaka et al. (2017) using observations from Japanese research institutes in the Pacific.
2. Evaluation of $NH_x(sw)$ sinks, i.e., nitrification, and uptake by plankton, against field observations. Critical uncertainties include the level of ammonium inhibition on nitrate uptake (Glibert et al., 2015) and the sensitivity of nitrification to the speciation of $NH_x(sw)$ (Beman et al., 2011; Ward, 2008).
3. Spatial pattern and sensitivity of nutrient limitation (Moore et al., 2013). In ESM4.1, increasing P limitation results in a large increase in NH_3 outgassing in coastal regions (+38%) and in the North Atlantic over the historical period.

4. Observations of gas-phase NH_3 in remote regions, which are needed to constrain the partitioning of NH_x between gas and aerosol phases. The impact of uncertainties in DMS emission and its response to climate change on the net outgassing of NH_3 also need to be better characterized.
5. Parameterization of NH_3 exchange (k_g) under extreme wind conditions (Johnson, 2010).
6. Quantification of the role of marine organic nitrogen as a source of marine NH_3. In particular, ESM4.1 remains unable to explain the large source of marine NH_3 reported by Altieri et al. (2014) in the outflow of North America, which suggests an important missing source of marine N.

Data Availability Statement

Observed NH_4^+ concentrations can be obtained at the CLIVAR and Carbon Hydrographic Data Office (https://cchdo.ucsd.edu/, last retrieved on 10 June 2019) and SeaDataNet (https://www.seadatanet.org/, last retrieved on 28 August 2019). ESM4.1 model outputs are available on the ESGF portal (John et al., 2018; Krasting et al., 2018).

Acknowledgments

We thank all our GFDL colleagues who made the GFDL-CM4 and ESM4.1 models possible. We thank Dr Vaishali Naik for processing CEDS emissions for use by GFDL models. We thank Dr John Dunne and two reviewers for their comments, which helped improve this manuscript.

References

Adcroft, A., Anderson, W., Balaji, V., Blanton, C., Bushuk, M., Dufour, C. O., et al. (2019). The GFDL global ocean and sea ice model OM4.0: Model description and simulation features. *Journal of Advances in Modeling Earth Systems*, *11*, 3167–3211. https://doi.org/10.1029/2019ms001726

Altieri, K. E., Fawcett, S. E., Peters, A. J., Sigman, D. M., & Hastings, M. G. (2016). Marine biogenic source of atmospheric organic nitrogen in the subtropical North Atlantic. *Proceedings of the National Academy of Sciences*, *113*(4), 925–930. https://doi.org/10.1073/pnas.1516847113

Altieri, K. E., Hastings, M. G., Peters, A. J., Oleynik, S., & Sigman, D. M. (2014). Isotopic evidence for a marine ammonium source in rainwater at Bermuda. *Global Biogeochemical Cycles*, *28*, 2014GB004809. https://doi.org/10.1002/2014GB004809

Anderson, L. A. (1995). On the hydrogen and oxygen content of marine phytoplankton. *Deep Sea Research Part I: Oceanographic Research Papers*, *42*(9), 1675–1680. https://doi.org/10.1016/0967-0637(95)00072-e

Beale, R., Johnson, M. T., Liss, P. S., & Nightingale, P. D. (2014). 8.3—air-sea exchange of marine trace gases. In H. D. H. K. Turekian (Ed.), *Treatise on geochemistry (second edition)* (pp. 53–92). Oxford: Elsevier.

Beman, J. M., Chow, C.-E., King, A. L., Feng, Y., Fuhrman, J. A., Andersson, A., et al. (2011). Global declines in oceanic nitrification rates as a consequence of ocean acidification. *Proceedings of the National Academy of Sciences of the United States of America*, *108*(1), 208–213.

Bouwman, A. F., Lee, D. S., Asman, W. A. H., Dentener, F. J., Van Der Hoek, K. W., & Olivier, J. G. J.(1997). A global high-resolution emission inventory for ammonia. *Global Biogeochemical Cycles*, *11*(4), 561–587.

Capotondi, A., Alexander, M. A., Bond, N. A., Curchitser, E. N., & Scott, J. D. (2012). Enhanced upper ocean stratification with climate change in the CMIP3 models. *Journal of Geophysical Research*, *117*, C04031. https://doi.org/10.1029/2011JC007409

Clegg, S. L., & Whitfield, M. (1995). A chemical model of seawater including dissolved ammonia and the stoichiometric dissociation constant of ammonia in estuarine water and seawater from −2 to 40°C. *Geochimica et Cosmochimica Acta*, *59*(12), 2403–2421. https://doi.org/10.1016/0016-7037(95)00135-2

Dortch, Q. (1990). The interaction between ammonium and nitrate uptake in phytoplankton. *Marine Ecology Progress Series*, *61*, 183–201.

Duce, R. A., LaRoche, J., Altieri, K., Arrigo, K. R., Baker, A. R., Capone, D. G., et al. (2008). Impacts of atmospheric anthropogenic nitrogen on the open ocean. *Science*, *320*(5878), 893.

Dunne, E. M., Gordon, H., Kurten, A., Almeida, J., Duplissy, J., Williamson, C., et al. (2016). Global atmospheric particle formation from CERN CLOUD measurements. *Science*, *354*(6316), 1119–1124. https://doi.org/10.1126/science.aaf2649

Dunne, J. P., Bociu, I., Bronselaer, B., Guo, H., John, J. G., Krasting, J. P., et al. (2020). Simple Global Ocean Biogeochemistry with Light, Iron, Nutrients and Gas version 2 (BLINGv2): Model description and simulation characteristics in GFDL's CM4.0. *Journal of Advances in Modeling Earth Systems*, *12*, e2019MS002008. https://doi.org/10.1029/2019MS002008

Fountoukis, C., & Nenes, A. (2007). ISORROPIA II: A computationally efficient thermodynamic equilibrium model for K^+–Ca^{2+}–Mg^{2+}–NH_4^+–Na^+–SO_4^{2-}–NO_3^-–Cl^-–H_2O aerosols. *Atmospheric Chemistry and Physics*, *7*(17), 4639–4659.

Frost, B. W., & Franzen, N. C. (1992). Grazing and iron limitation in the control of phytoplankton stock and nutrient concentration: A chemostat analogue of the pacific equatorial upwelling zone. *Marine Ecology Progress Series*, *83*(2), 291–303.

Fujimori, S., Hasegawa, T., Masui, T., Takahashi, K., Herran, D. S., Dai, H., et al. (2017). SSP3: AIM implementation of shared socioeconomic pathways. *Global Environmental Change*, *42*, 268–283. https://doi.org/10.1016/j.gloenvcha.2016.06.009

Geider, R. J., MacIntyre, H. L., & Kana, T. M. (1997). Dynamic model of phytoplankton growth and acclimation: Responses of the balanced growth rate and the chlorophyll a: Carbon ratio to light, nutrient-limitation and temperature. *Marine Ecology Progress Series*, *148*, 187–200. https://doi.org/10.3354/meps148187

Gibb, S. W., Mantoura, R. F. C., & Liss, P. S. (1999). Ocean-atmosphere exchange and atmospheric speciation of ammonia and methylamines in the region of the NW Arabian Sea. *Global Biogeochemical Cycles*, *13*(1), 161–178.

Glibert, P. M., Wilkerson, F. P., Dugdale, R. C., Raven, J. A., Dupont, C. L., Leavitt, P. R., et al. (2015). Pluses and minuses of ammonium and nitrate uptake and assimilation by phytoplankton and implications for productivity and community composition, with emphasis on nitrogen-enriched conditions. *Limnology and Oceanography*, *61*(1), 165–197. https://doi.org/10.1002/lno.10203

Gruber, N. (2008). *The marine nitrogen cycle: Overview and challenges* (Second). In D. G. Capone, D. A. Bronk, M. R. Mulholland, & E. J. Carpenter (Eds.). Amsterdam: Academic Press.

Hoesly, R. M., Smith, S. J., Feng, L., Klimont, Z., Janssens-Maenhout, G., Pitkanen, T., et al. (2018). Historical (1750–2014) anthropogenic emissions of reactive gases and aerosols from the community emissions data system (ceds). *Geoscientific Model Development*, *11*(1), 369–408. https://doi.org/10.5194/gmd-11-369-2018

Hopkins, F. E., Suntharalingam, P., Gehlen, M., Andrews, O., Archer, S. D., Bopp, L., et al. (2020). The impacts of ocean acidification on marine trace gases and the implications for atmospheric chemistry and climate. *Proceedings of the Royal Society A: Mathematical, Physical and Engineering Sciences*, *476*(2237), 20190769. https://doi.org/10.1098/rspa.2019.0769

Horowitz, L. W., Naik, V., Paulot, F., Ginoux, P. A., Dunne, J. P., Mao, J., et al. (2020). The GFDL Global Atmospheric Chemistry-Climate Model AM4.1: Model Description and Simulation Characteristics. *Journal of Advances in Modeling Earth Systems*, *12*, e2019MS002032. https://doi.org/10.1029/2019MS002032

Huesemann, M. H., Skillman, A. D., & Crecelius, E. A. (2002). The inhibition of marine nitrification by ocean disposal of carbon dioxide. *Marine Pollution Bulletin*, *44*(2), 142–148. https://doi.org/10.1016/s0025-326x(01)00194-1

Jacobson, M. Z. (2005). *Fundamentals of atmospheric modeling*. Cambridge: Cambridge University Press. https://doi.org/10.1017/cbo9781139165389

Jeandel, C., Ruiz-Pino, D., Gjata, E., Poisson, A., Brunet, C., Charriaud, E., et al. (1998). KERFIX, a time-series station in the southern ocean: A presentation. *Journal of Marine Systems*, *17*(1–4), 555–569. https://doi.org/10.1016/s0924-7963(98)00064-5

Jickells, T. D., Buitenhuis, E., Altieri, K., Baker, A. R., Capone, D., Duce, R. A., et al. (2017). A reevaluation of the magnitude and impacts of anthropogenic atmospheric nitrogen inputs on the ocean. *Global Biogeochemical Cycles*, *31*, 289–305. https://doi.org/10.1002/2016GB005586

Jickells, T. D., Kelly, S. D., Baker, A. R., Biswas, K., Dennis, P. F., Spokes, L. J., et al. (2003). Isotopic evidence for a marine ammonia source. *Geophysical Research Letters*, *30*, 1374. https://doi.org/10.1029/2002GL016728

John, J. G., Blanton, C., McHugh, C., Nikonov, S., Radhakrishnan, A., Rand, K., et al. (2018). NOAA-GFDL GFDL-ESM4 model output prepared for CMIP6 ScenarioMIP. Earth System Grid Federation. https://doi.org/10.22033/ESGF/CMIP6.1414

Johnson, M. T. (2010). A numerical scheme to calculate temperature and salinity dependent air-water transfer velocities for any gas. *Ocean Science*, *6*(4), 913–932.

Johnson, M. T., Liss, P. S., Bell, T. G., Lesworth, T. J., Baker, A. R., Hind, A. J., et al. (2008). Field observations of the ocean-atmosphere exchange of ammonia: Fundamental importance of temperature as revealed by a comparison of high and low latitudes. *Global Biogeochemical Cycles*, *22*, GB1019. https://doi.org/10.1029/2007GB003039

Johnson, M. T., Sanders, R., Avgoustidi, V., Lucas, M., Brown, L., Hansell, D., et al. (2007). Ammonium accumulation during a silicate-limited diatom bloom indicates the potential for ammonia emission events. *Marine Chemistry*, *106*(1–2), 63–75.

Jokinen, T., Sipilä, M., Kontkanen, J., Vakkari, V., Tisler, P., Duplissy, E.-M., et al. (2018). Ion-induced sulfuric acid–ammonia nucleation drives particle formation in coastal antarctica. *Science Advances*, *4*(11), eaat9744. https://doi.org/10.1126/sciadv.aat9744

Kamezaki, K., Hattori, S., Iwamoto, Y., Ishino, S., Furutani, H., Miki, Y., et al. (2019). Tracing the sources and formation pathways of atmospheric particulate nitrate over the pacific ocean using stable isotopes. *Atmospheric Environment*, *209*, 152–166. https://doi.org/10.1016/j.atmosenv.2019.04.026

Kanakidou, M., Duce, R. A., Prospero, J. M., Baker, A. R., Benitez-Nelson, C., Dentener, F. J., et al. (2012). Atmospheric fluxes of organic n and p to the global ocean. *Global Biogeochemical Cycles*, *26*, GB3026. https://doi.org/10.1029/2011GB004277

Kaufmann, P., Fundel, F., Fischer, H., Bigler, M., Ruth, U., Udisti, R., et al. (2010). Ammonium and non-sea salt sulfate in the EPICA ice cores as indicator of biological activity in the southern ocean. *Quaternary Science Reviews*, *29*(1–2), 313–323.

Kim, T.-W., Lee, K., Duce, R., & Liss, P. (2014). Impact of atmospheric nitrogen deposition on phytoplankton productivity in the South China Sea. *Geophysical Research Letters*, *41*, 3156–3162. https://doi.org/10.1002/2014GL059665

Kim, I.-N., Lee, K., Gruber, N., Karl, D. M., Bullister, J. L., Yang, S., & Kim, T.-W. (2014). Increasing anthropogenic nitrogen in the North Pacific Ocean. *Science*, *346*(6213), 1102–1106. https://doi.org/10.1126/science.1258396

Kim, T.-W., Lee, K., Najjar, R. G., Jeong, H.-D., & Jeong, H. J. (2011). Increasing N abundance in the Northwestern Pacific Ocean due to atmospheric nitrogen deposition. *Science*, *334*(6055), 505–509.

Kirkby, J., Curtius, J., Almeida, J., Dunne, E., Duplissy, J., Ehrhart, S., et al. (2011). Role of sulphuric acid, ammonia and galactic cosmic rays in atmospheric aerosol nucleation. *Nature*, *476*(7361), 429–433.

Kitidis, V., Laverock, B., McNeill, L. C., Beesley, A., Cummings, D., Tait, K., et al. (2011). Impact of ocean acidification on benthic and water column ammonia oxidation. *Geophysical Research Letters*, *38*, L21603. https://doi.org/10.1029/2011GL049095

Krasting, J. P., John, J. G., Blanton, C., McHugh, C., Nikonov, S., Radhakrishnan, A., et al. (2018). NOAA-GFDL GFDL-ESM4 model output prepared for CMIP6 CMIP. Earth System Grid Federation. https://doi.org/10.22033/ESGF/CMIP6.1407

Krishnamurthy, A., Moore, J. K., Mahowald, N., Luo, C., Doney, S. C., Lindsay, K., & Zender, C. S.(2009). Impacts of increasing anthropogenic soluble iron and nitrogen deposition on ocean biogeochemistry. *Global Biogeochemical Cycles*, *23*, GB3016. https://doi.org/10.1029/2008GB003440

Krishnamurthy, A., Moore, J. K., Mahowald, N., Luo, C., & Zender, C. S. (2010). Impacts of atmospheric nutrient inputs on marine biogeochemistry. *Journal of Geophysical Research*, *115*, G01006. https://doi.org/10.1029/2009JG001115

Krishnamurthy, A., Moore, J. K., Zender, C. S., & Luo, C. (2007). Effects of atmospheric inorganic nitrogen deposition on ocean biogeochemistry. *Journal of Geophysical Research*, *112*, G02019. https://doi.org/10.1029/2006JG000334

Legrand, M., Ducroz, F., Wagenbach, D., Mulvaney, R., & Hall, J. (1998). Ammonium in coastal antarctic aerosol and snow: Role of polar ocean and penguin emissions. *Journal of Geophysical Research*, *103*(D9), 11,043–11,056.

Letscher, R. T., Primeau, F., & Moore, J. K. (2016). Nutrient budgets in the subtropical ocean gyres dominated by lateral transport. *Nature Geoscience*, *9*(11), 815–819. https://doi.org/10.1038/ngeo2812

Liss, P. S., & Slater, P. G. (1974). Flux of gases across the air-sea interface. *Nature*, *247*(5438), 181–184.

Martiny, A. C., Lomas, M. W., Fu, W., Boyd, P. W., Ling, L., Chen, Y., et al. (2019). Biogeochemical controls of surface ocean phosphate. *Science Advances*, *5*(8), eaax0341. https://doi.org/10.1126/sciadv.aax0341

Moore, C. M., Mills, M. M., Arrigo, K. R., Berman-Frank, I., Bopp, L., Boyd, P. W., et al. (2013). Processes and patterns of oceanic nutrient limitation. *Nature Geoscience*, *6*(9), 701–710.

Naik, V., Horowitz, L. W., Fiore, A. M., Ginoux, P., Mao, J., Aghedo, A. M., & Levy, H. (2013). Impact of preindustrial to present-day changes in short-lived pollutant emissions on atmospheric composition and climate forcing. *Journal of Geophysical Research: Atmospheres*, *118*, 8086–8110. https://doi.org/10.1002/jgrd.50608

O'Neill, R. V., DeAngelis, D. L., Pastor, J. J., Jackson, B. J., & Post, W. M. (1989). Multiple nutrient limitations in ecological models. *Ecological Modelling*, *46*(3–4), 147–163. https://doi.org/10.1016/0304-3800(89)90015-x

Paulot, F., Ginoux, P., Cooke, W. F., Donner, L. J., Fan, S., Lin, M.-Y., et al. (2016). Sensitivity of nitrate aerosols to ammonia emissions and to nitrate chemistry: Implications for present and future nitrate optical depth. *Atmospheric Chemistry and Physics*, *16*(3), 1459–1477.

Paulot, F., Jacob, D. J., Johnson, M. T., Bell, T. G., Baker, A. R., Keene, W. C., et al. (2015). Global oceanic emission of ammonia: Constraints from seawater and atmospheric observations. *Global Biogeochemical Cycles*, *29*, 1165–1178. https://doi.org/10.1002/2015GB005106/full

Peng, X., Fuchsman, C. A., Jayakumar, A., Warner, M. J., Devol, A. H., & Ward, B. B. (2016). Revisiting nitrification in the eastern tropical south pacific: A focus on controls. *Journal of Geophysical Research: Oceans*, *121*, 1667–1684. https://doi.org/10.1002/2015JC011455

Quinn, P. K., Asher, W. E., & Charlson, R. J. (1992). Equilibria of the marine multiphase ammonia system. *Journal of Atmospheric Chemistry*, *14*(1–4), 11–30.

Quinn, P. K., Barrett, K. J., Dentener, F. J., Lipschultz, F., & Six, K. D. (1996). Estimation of the air/sea exchange of ammonia for the North Atlantic basin. *Biogeochemistry*, *35*(1), 275–304.

Ren, H., Chen, Y.-C., Wang, X. T., Wong, G. T. F., Cohen, A. L., DeCarlo, T. M., et al. (2017). 21st-century rise in anthropogenic nitrogen deposition on a remote coral reef. *Science*, *356*(6339), 749–752. https://doi.org/10.1126/science.aal3869

Riddick, S. N., Dragosits, U., Blackall, T. D., Daunt, F., Wanless, S., & Sutton, M. A. (2012). The global distribution of ammonia emissions from seabird colonies. *Atmospheric Environment*, *55*, 319–327.

Sarmiento, J. L., & Gruber, N. (2013). *Ocean biogeochemical dynamics*. Princeton: Princeton University Press.

Seitzinger, S. P., Harrison, J. A., Dumont, E., Beusen, A. H. W., & Bouwman, A. F. (2005). Sources and delivery of carbon, nitrogen, and phosphorus to the coastal zone: An overview of global nutrient export from watersheds (NEWS) models and their application. *Global Biogeochemical Cycles*, *19*, GB4S01. https://doi.org/10.1029/2005GB002606

Sherman, K., & Alexander, L. (1986). *Variability and management of large marine ecosystems*. Boulder: Westview Press.

Smith, B., Wårlind, D., Arneth, A., Hickler, T., Leadley, P., Siltberg, J., & Zaehle, S. (2014). Implications of incorporating N cycling and N limitations on primary production in an individual-based dynamic vegetation model. *Biogeosciences*, *11*(7), 2027–2054. https://doi.org/10.5194/bg-11-2027-2014

St-Laurent, P., Friedrichs, M. A. M., Najjar, R. G., Martins, D. K., Herrmann, M., Miller, S. K., & Wilkin, J. (2017). Impacts of atmospheric nitrogen deposition on surface waters of the western North Atlantic mitigated by multiple feedbacks. *Journal of Geophysical Research: Oceans*, *122*, 8406–8426. https://doi.org/10.1002/2017JC013072

Stein, L. Y., Arp, D. J., & Hyman, M. R. (1997). Regulation of the synthesis and activity of ammonia monooxygenase in Nitrosomonas europaea by altering pH to affect NH(inf3) availability. *Applied and Environmental Microbiology*, *63*(11), 4588–4592.

Stock, C. A., Dunne, J. P., Fan, S., Ginoux, P., John, J., Krasting, J. P., et al. (2020). Ocean Biogeochemistry in GFDL's Earth System Model 4.1 and its response to increasing atmospheric CO_2. *Journal of Advances in Modeling Earth Systems*, *12*, e2019MS002043. https://doi.org/10.1029/2019MS002043

Stock, C. A., Dunne, J. P., & John, J. G. (2014a). Drivers of trophic amplification of ocean productivity trends in a changing climate. *Biogeosciences*, *11*(24), 7125–7135.

Stock, C. A., Dunne, J. P., & John, J. G. (2014b). Global-scale carbon and energy flows through the marine planktonic food web: An analysis with a coupled physical-biological model. *Progress in Oceanography*, *120*(0), 1–28.

Suzuki, I., Dular, U., & Kwok, S. C. (1974). Ammonia or ammonium ion as substrate for oxidation by Nitrosomonas europaea cells and extracts. *Journal of Bacteriology*, *120*(1), 556–558.

Syrett, P. J. (1981). In T. Platt (Ed.), *Nitrogen metabolism of microalgea* (Vol. 210). Ottawa: Canadian Bulletin of Fisheries and Aquatic Sciences.

van Marle, M. J. E., Kloster, S., Magi, B. I., Marlon, J. R., Daniau, A.-L., Field, R. D., et al. (2017). Historic global biomass burning emissions for CMIP6 (BB4CMIP) based on merging satellite observations with proxies and fire models (1750–2015). *Geoscientific Model Development*, *10*(9), 3329–3357. https://doi.org/10.5194/gmd-10-3329-2017

Wang, X. T., Cohen, A. L., Luu, V., Ren, H., Su, Z., Haug, G. H., & Sigman, D. M. (2018). Natural forcing of the North Atlantic nitrogen cycle in the Anthropocene. *Proceedings of the National Academy of Sciences*, *115*(42), 10,606–10,611. https://doi.org/10.1073/pnas.1801049115

Wang, W.-L., Moore, J. K., Martiny, A. C., & Primeau, F. W. (2019). Convergent estimates of marine nitrogen fixation. *Nature*, *566*(7743), 205–211. https://doi.org/10.1038/s41586-019-0911-2

Ward, B. B. (2008). Nitrification in marine systems. *Nitrogen in the marine environment* (pp. 199–261). Amsterdam: Elsevier. https://doi.org/10.1016/b978-0-12-372522-6.00005-0

Ward, B. B., Olson, R. J., & Perry, M. J. (1982). Microbial nitrification rates in the primary nitrite maximum off Southern California. *Deep Sea Research II*, *29*(2), 247–255.

Yang, S., & Gruber, N. (2016). The anthropogenic perturbation of the marine nitrogen cycle by atmospheric deposition: Nitrogen cycle feedbacks and the 15 n Haber-Bosch effect. *Global Biogeochemical Cycles*, *30*, 1418–1440. https://doi.org/10.1002/2016GB005421

Yasunaka, S., Nojiri, Y., Hashioka, T., Yoshikawa, C., Kodama, T., Ichiro Nakaoka, S., et al. (2017). Basin-scale distribution of NH_4^+ and NO_2^- in the pacific ocean. *Journal of Oceanography*, *74*(1), 1–11. https://doi.org/10.1007/s10872-017-0433-1

Zhang, Q., & Anastasio, C. (2003). Conversion of fogwater and aerosol organic nitrogen to ammonium, nitrate, and NO_x during exposure to simulated sunlight and ozone. *Environmental Science & Technology*, *37*(16), 3522–3530.

Zhao, M., Golaz, J.-C., Held, I. M., Guo, H., Balaji, V., Benson, R., et al. (2018). The GFDL global atmosphere and land model AM4.0/LM4.0 - 1. simulation characteristics with prescribed SSTs. *Journal of Advances in Modeling Earth Systems*, *10*, 691–734. https://doi.org/10.1002/2017MS001208